











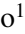



Ingot-like class of wavefront sensors for laser guide stars

R. Ragazzoni^{1,2,6} , E. Portaluri^{3,6} , D. Greggio^{2,6} , M. Dima^{2,6}, C. Arcidiacono^{2,6} , M. Bergomi^{2,6} ,
S. Di Filippo^{2,6} , T. S. Gomes Machado^{1,2,6} , K. K. R. Santhakumari^{2,6} , V. Viotto^{2,6} , F. Battaini^{2,6} ,
E. Carolo^{2,6} , S. Chinellato^{2,6}, J. Farinato^{2,6}, D. Magrin^{2,6} , L. Marafatto^{2,6},
G. Umbriaco^{1,4,5,6} , and D. Vassallo^{2,6} 

¹ Dipartimento di Fisica e Astronomia “G. Galilei”, Università di Padova, vicolo dell’Osservatorio 3, 35122 Padova, Italy
e-mail: roberto.ragazzoni@unipd.it

² INAF – Osservatorio Astronomico di Padova, vicolo dell’Osservatorio 5, 35122 Padova, Italy

³ INAF – Osservatorio Astronomico d’Abruzzo, via Mentore Maggini snc, 64100 Teramo, Italy

⁴ Dipartimento di Fisica e Astronomia “A. Righi” – Alma Mater Studiorum Università di Bologna, via Piero Gobetti 93/2, 40129 Bologna, Italy

⁵ INAF – Osservatorio di Astrofisica e Scienza dello Spazio, via Gobetti 93/3, 40129 Bologna, Italy

⁶ ADONI – Laboratorio Nazionale Ottiche Adattive, Italy

Received 22 February 2024 / Accepted 23 May 2024

ABSTRACT

Context. Full sky coverage adaptive optics (AO) on extremely large telescopes requires the adoption of several laser guide stars as references. With such large apertures, the apparent elongation of the beacons is absolutely significant. With a few exceptions, wavefront sensors (WFSs) designed for natural guide stars can be adapted and used in suboptimal mode in this context.

Aims. We analyse and describe the geometrical properties of a class of WFSs that are specifically designed to deal with laser guide stars propagated from a location in the immediate vicinity of the telescope aperture.

Methods. We describe, in three dimensions, the loci where the light of the laser guide stars would focus in the focal volume located behind the focal plane where astronomical objects are reimaged. We also describe the properties of several types of optomechanical devices that act as perturbers for this new class of pupil plane sensors, through refraction and reflections. We refer to these as ingot WFSs.

Results. We provide the recipes both for the most reasonably complex version of these WFSs, with six pupils and, for the simplest one, only three pupils. Both of them are referred to on the basis of the European Extremely Large Telescope (ELT) case. We outlined elements that are meant to give a qualitative idea of how the sensitivity of this new class of sensors compares to conventional ones.

Conclusions. We present a new class of WFSs, based on an extension to the case of elongated sources at a finite distance of the pyramid WFS. We point out which advantages of the pyramid can be retained and how it may be adopted to optimize the sensing procedure.

Key words. instrumentation: adaptive optics

1. Introduction

Adaptive optics (AO) allows us to achieve diffraction-limited imaging on large ground-based telescopes (Tyson 1991; Beckers 1993; Hardy 1998). It can be characterized in terms of achieved performances based on three parameters. The first one represents the degree of the achieved compensation, often indicated by the ratio of the peak of the compensated point spread function (PSF) of an unresolved source to the diffraction limit one, the so-called Strehl ratio (Strehl 1895; Herrmann 1992). This compensation ranges from seeing amelioration (Rigaut 2002; Tokovinin 2004), to modest Strehl ratios, up to the extreme AO case that is encompassed by high-contrast system, usually aimed at the detection of circumstellar or exoplanets around bright stars (Macintosh 2001; Esposito et al. 2003, 2010; Guyon 2018) and limited to a very narrow field of view (FoV). The second parameter is, in fact, the size of such a compensated FoV that is naturally limited to the isoplanatic patch in the case where a single conjugated AO is achieved. Multiple correctors in a large variety of configurations both for compensation and sensing have been described (Dicke 1975; Beckers 1988; Ellerbroek 1994; Ragazzoni et al. 2000a,

2002; Ragazzoni 2014; Rigaut & Neichel 2018) and some tested on sky to date (Marchetti et al. 2003, 2008; Rigaut et al. 2014; Neichel et al. 2014; Herbst et al. 2018). Finally, the third fundamental parameter is the sky-coverage, the fraction of the sky where the compensation can actually be achieved.

The sky coverage issue has been addressed by conceiving AO systems that can work with rather faint reference sources, eventually scattered in a large area in the sky (Ragazzoni et al. 2013; Viotto et al. 2015; Portaluri et al. 2017) or by producing artificial reference sources by propagating light beams from the ground (Thompson & Gardner 1987; Rigaut et al. 2014) and sensing the signal provided by some of the returning light by means of different processes, such as Rayleigh (Foy & Labeyrie 1985) or resonant scattering (Pilkington 1987).

Sodium laser guide stars (LGSs) have become routinely available in a few observatories (Rigaut et al. 2014; Calia et al. 2014; D’Orgeville & Fetzer 2016) also in multiple formats (possibly forming true artificial asterisms) and are usually considered as the obvious solution to the sky coverage issue. While the AO system that first reliably and consistently used these artificially generated beacons succeeded in producing unique science

(Genzel et al. 2003; Ghez et al. 2008), it is remarkable to note that anyhow they would rely on some natural guide stars (NGSs) because of the lack of determination with respect to the absolute position in the sky of the artificial reference due to the upward turbulence encountered by the light propagating from the ground to the sky (Rigaut & Gendron 1992; Foy et al. 1995; Ragazzoni 1996a, 1997, 2000; Esposito et al. 2000).

Assuming the availability of the desired return flux from these LGSs, their associated wavefront sensor (WFS) is not necessarily have to be characterized by any minimum efficiency. In fact, the current examples of AO systems encompassing LGSs are just conventional types of WFSs, usually conceived for NGSs, that have been adapted to the location and wavelength of these peculiar references.

However, these sources (from an optical viewpoint), despite their being referred to as “stars”, they are actually unresolved sources located at an infinite distance, akin to that of an NGS. On top of the obvious evidence that they are located at a finite distance (typically at 92 km of height, corresponding to a continuously changing range that depends upon the zenith distance at which the observation is carried out), they have a non-negligible distribution in all spatial dimensions, especially along the laser’s line of propagation, which is not necessarily co-aligned with the line of sight.

The departure of the appearance of the LGSs from an NGS (provided proper refocussing is done) is somehow proportional to the diameter of the observing telescope, so that this issue has minimal impact on current 8 to 10 m state of the art class telescopes; however, it is expected to play a more significant role in the future gigantic ground based optical telescopes such as European Extremely Large Telescope (ELT, Gilmozzi & Spyromilio 2007), Giant Magellan Telescope (GMT, Johns 2008), and Thirty Meter Telescope (TMT, Szeto et al. 2008). Two of the most prominent instruments on those telescopes will make use of LGS-adopted Shack–Hartmann (SH) WFS, as a well consolidated (albeit likely suboptimal) technology (Boyer & Ellerbroek 2016; Agapito et al. 2022).

The paper is organized as follows. In Sect. 2, we describe the geometry of the LGS, including the relationships between the source and the elongated spot on the focal volume. Section 3 explores the several possible options for the new class of WFSs, combining reflecting and refracting surfaces. It provides a geometric description of the WFS (Sect. 3.1) and focuses on two extreme realizations with six (Sect. 3.2) and three pupils (Sect. 3.3). Section 4 provides a summary and conclusion.

2. Description of the LGS in the focal volume

Treating the LGSs as a cylindrical emitting volume rather than point sources reveals several suboptimal characteristics in the associated WFS. This leads to an increase in the required returning flux to attain a certain level of accuracy.

Most of the literature has dealt with the apparent angular spreading of LGSs (called elongation), managing a number of countermeasures or specific technical issues, such as the truncation of its image when treated by a classical WFS (Diolaiti et al. 2012; Schreiber et al. 2014; Vieira et al. 2018; Clare et al. 2020).

In principle, the conceptual design of a WFS could incorporate the way this light is produced, tailoring that specific need and thereby becoming a more efficient method than merely treating LGSs as stars (Ragazzoni et al. 2017). Some of these approaches have been described in the literature: the z -invariant WFS (Ragazzoni et al. 2001), the Projected Pupil Plane Pattern (PPPP) concept (Buscher et al. 2002; Yang et al. 2018),

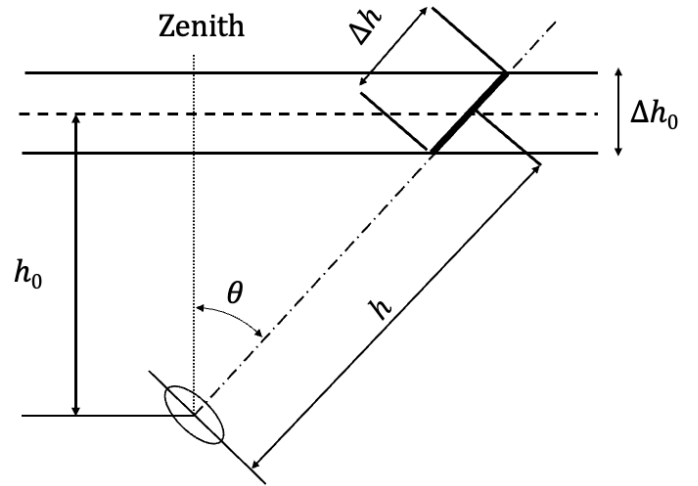


Fig. 1. Geometry of the launching of a mesospheric sodium layer LGS. In this schematic view, the layer is approximated with a solid bandwagon of a thickness, Δh , located at an averaged height, h_0 . The curvature of the Earth is considered negligible, making the zenith distance, θ , the only parameter required to retrieve the equivalent range of h and the apparent thickness, Δh .

Sky-Projected Laser Array Shack–Hartmann (SPLASH) (Butterley et al. 2006), the CAFADIS camera (Rodríguez-Ramos et al. 2008), the Plenoptic WFS (Zhang et al. 2021), or through a smart optical arrangements of the SH beams (Lombini et al. 2022). Some configurations have been arranged on a laboratory breadboard, where the overall configuration is scaled down to a laboratory size (Yang et al. 2019). Finally, some of them have been tested, albeit with some limitations (Bharmal et al. 2018) and on the sky (Ragazzoni et al. 2006).

We extend now one of these earliest concept, namely the roof-like WFS (Ragazzoni 2001), customizing it to the sodium LGSs and extending its ability to provide information in both the directions: the orthogonal one and the one aligned with respect to the apparent elongation of the sodium beacon as seen from the main aperture of the telescope.

We start by considering a laser tuned to the proper sodium doublet wavelengths propagating the beam through a projector producing an LGS at a zenith distance θ (Fig. 1). The sodium layer, located at an altitude of h_0 and nominal thickness of Δh_0 will be seen from the launching area at a range, h , and with an equivalent projected thickness, Δh , given by:

$$h = \frac{h_0}{\cos \theta}; \quad \Delta h = \frac{\Delta h_0}{\cos \theta}. \quad (1)$$

Each point of the sodium column emitting light will appear with an apparent defocus if observed on the nominal focal plane at which objects at infinity are conjugated.

If the equivalent focal length of the telescope is f , with F as the focal ratio of the optical system and D its aperture, we may note that a point C located in the nominal range at the sodium layer will be reimaged well behind the focal plane where astronomical objects are focused (Fig. 2). The detailed position is indicated by h' and s' under the conditions that the LGS is being propagated from a projector located at a distance s from the center and on the plane of the telescope pupil O , and (only for the sake of this preliminary discussion) the propagation of the LGS will be parallel to the optical axis of the telescope. In this configuration and using the thin-lens approximation, it is

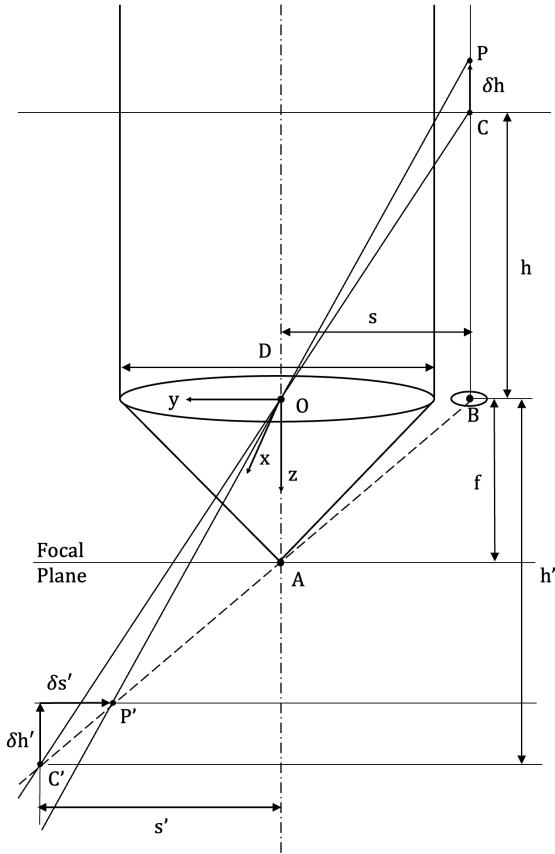


Fig. 2. Geometry describing the reimaging of a vertically extended LGS beacon projected from outside the telescope pupil and co-aligned with its optical axis. Points P and C of the LGS are reimaged onto P' and C' that are aligned with A and B , which are the focus of an on-axis astronomical source and the center of the LGS projector, respectively.

possible to figure out the distance along the optical axis of the reimaged position of the point C' . The axial distance is given by:

$$h' = \frac{fh}{h-f}. \quad (2)$$

This relationship, whenever $f \ll h$ (a condition generally well accomplished), can be approximated by the following:

$$h' \approx f + \frac{f^2}{h}. \quad (3)$$

Similarly, the lateral displacement with respect to the optical axis of the imaged point C' can be figured out by using the similarity of the proper triangles having a common vertex in the center of the telescope pupil O , through the following relationship:

$$\frac{s'}{h'} = \frac{s}{h}, \quad (4)$$

which fully characterizes the position of C' . As the LGS extends along the direction of propagation of the laser beam, we can go on to work out the effects of a relatively small displacement from the starting point C , namely to a generic point P located at a displaced distance from the laser beam by a (small) amount δh typically lying in the range $\pm \Delta h/2$.

In particular, we can rewrite Eq. (2) by replacing the displaced position of the reimaged point P' as:

$$h' - \delta h' = \frac{f(h + \delta h)}{h + \delta h - f}. \quad (5)$$

Under the reasonable assumption that both $f, \delta h \ll h$ and using also Eq. (3), one can rewrite it into the following:

$$\frac{\delta h}{\delta h'} \approx \frac{h^2}{f^2}. \quad (6)$$

We can obtain an equivalent relationship to Eq. (4), using the similarity of the angles having as vertexes P and P' and, again, common vertex in the center of the telescope pupil, as:

$$\frac{s' - \delta s'}{h' - \delta h'} = \frac{s}{h + \delta h}. \quad (7)$$

After a tedious but straightforward rearrangement using sequentially the results given by Eqs. (5), (6), and (2), while also adopting the mentioned approximation, we can finally express:

$$\frac{\delta s'}{\delta h'} \approx \frac{s}{f}. \quad (8)$$

It is interesting that this result indicates that the locus of the points where the image of the elongated LGS is lying can be described as a segment. Such pattern is inclined with respect to the optical axis in a manner that, if prolonged, will hit both the nominal focus of an infinite distant on axis source and the position, along the plane of the pupil, where the beam is propagated (see the dashed line in Fig. 2). In other words, within such an approximation, this finding leads to the consequence that the triangles with hypotenuses $\overline{C'P'}$ and \overline{AB} are similar. This is the so-called Scheimpflug principle (Scheimpflug 1904; Mayer 1994), which can be geometrically explained by extending the power of the telescope outside of its nominal diameter up to reach the LGS projector and using the geometric approximation of the thin lenses to figure out the reimaged points along the LGS beam. The Scheimpflug principle can be applied to any direction of propagation of the LGS angles φ and ω , as shown in Fig. 3.

As a consequence, when the LGS projector is located outside of the telescope pupil, the illuminating beams will never embed the LGS image itself. On the contrary, in the case of a LGS propagated from behind the cage of a secondary mirror, in a typical two-mirror telescope, the locus where the LGS image is in focus lies within the beams coming from other portions of the LGS. This has nothing to do with the fratricide effect (Gratadour et al. 2010), which is related to the augmented background due to the light scattered from the LGS itself. For this reason, the class of WFSs presented in this paper is suitable only to those telescopes in which the LGS projector is placed outside of the telescope pupil as will be evident in the following section.

3. Toward a new class of WFSs

The whole light emitted by the LGS can be subdivided in different regions, with the aim of gathering information on how the light has been perturbed by the atmosphere. This can be accomplished by reflecting or refracting interfaces that would bend the incoming beam, which will then be recollected by a common pupil imager, to form a sort of pupil-plane WFS tailored to the specific case of LGSs. This type of WFS garnered attention in recent decades, mainly because of its high sensitivity. It

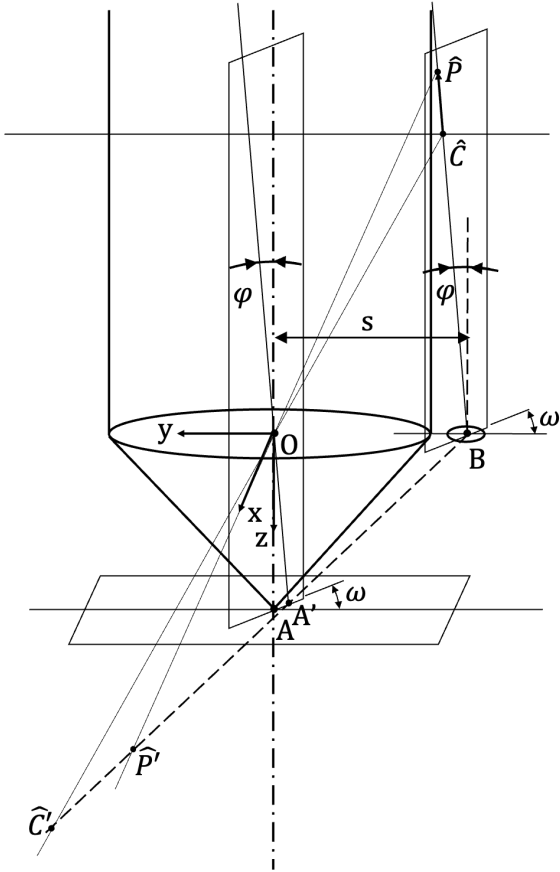


Fig. 3. Scheimpflug principle applied to a generic position, defined by the angles φ and ω , and line of sight of the LGS projector. In this case, the alignment between \hat{C} and \hat{P} and B intersects the nominal focal plane for astronomical objects in the point A' . This is where an astronomical source located in the direction of the LGS will focus.

includes an optomechanical device located in the focal volume and a reimager of the pupil plane. The term “pupil-plane” refers to the location where the detector is placed (see, e.g., Horwitz 1994; Ma & Wang 2016). A detailed description and a list of this category of WFSs can also be found in Ragazzoni et al. (2019).

Because of the solid shape, in this case, such a reflective and refractive device combination resembles the surfaces of an ingot (hence, the nickname given to this class of WFSs). In the following, we describe how we established a coordinate system, whereby the origin, O , is located in the center of the entrance pupil of the main telescope; the z axis is deployed along its optical axis in a positive sense toward the focal plane; the y axis defines the location where the LGS projector is located (at position $y = -s$) such that (generally speaking) the image of the LGS falls at positive values of y ; finally, the x axis is added in order to be arranged in a normal Cartesian coordinate system.

In a similar fashion to the way different types of pupil illumination are used to sense the derivative of the wavefront (Ragazzoni 1996b), in two dimensions in the pyramid WFS, these multi-faceted prisms would produce a corresponding number of pupil images to be used for similar purposes. In this way, we can efficiently measure the derivative of the wavefront along the x -axis by combining all the pupils collecting the light from the whole of the LGS, and the derivative of the wavefront along the y -axis using the light coming from the endpoints of the LGS. A crude version of this approach, solely suited to identify the derivative along the x -axis of a Rayleigh reference beacon,

appeared in Ragazzoni et al. (2000b). In that context, no attempt was made for measuring the derivative along the y -axis, given the fact that such references are characterized by a vanishing or non-existing edge along the direction of propagation.

The case of the conventional pyramid WFS used with LGS is not treated in details here, however, as it deals with sources much larger than the diffraction limit ones in all dimensions (including the one orthogonal to the elongation), it can be regarded as a sub case of a SH with a 2×2 pixels per subaperture; hence, including a very large oversampling of the LGS image. It is also fair to point out that one of the key features of the pyramid WFS, namely, the enhanced sensitivity reached in a closed loop (Ragazzoni & Farinato 1999), is not achievable here. This is because the LGS is usually much larger than the diffraction limit of the telescope, so the closed loop operations do not change significantly its apparent size and they cannot be used to retrieve any useful information. The only way to retain such a feature would be by producing an LGS whose apparent size, other than the elongation, is comparable to the diffraction limit of the telescope. This can be accomplished by propagating the LGS through a similarly sized aperture, with the additional incumbency of compensating for the upward atmospheric turbulence (Esposito & Busoni 2008). Practically, this can be obtained efficiently only using the same telescope aperture as a laser projector, with the obvious associated complexity of achieving such a task (Fugate et al. 1994; Wilson et al. 1997). For these reasons, such a possibility is not further elaborated upon in this work.

To obtain a similar behaviour on a SH WFS, we should account for the largest number of pixels required at the subapertures that are more distant than where the LGS is being propagated. This would require an overall very large number of pixels, which would be almost unused in the regions close to where the LGS is being propagated, where the apparent elongation is small.

The overall number of regions subdividing the LGS image each (producing a pupil image) can be, in principle, as large as desired, provided that practical issues are taken into account. For instance, a minimum requirement for this approach is that the bending angles are such that the commonly reimaged pupils do not end up superimposed. This fact translates into the condition that the bending angles are at least the angle defined by the marginal rays of the converging beams, amounting to the inverse of the focal ratio at the LGS image position (Fig. 4). Moreover, a large number of pupil images will require larger bending angles, corresponding to a larger FoV capability of the collimating system.

We believe that once we relinquish the use of the structure of the brightness along the LGS, the maximum reasonable number of regions is six (Ragazzoni et al. 2018). This is the case depicted in Fig. 4 and in the first case of Fig. 5. There are, however, a number of interesting features that are common to all the versions of WFSs that are described in this work. The distribution of light in points of the pupil that experience different elongations reflects the availability of the light for sensing the derivative of the wavefront in different directions. In other words, points closer to the location where the LGS is propagated will see the WFS as a nearly pyramid one (with only, or mainly, four faces in the most complete case). Instead, when the largest elongation occurs, the largest fraction of the light is only used for sensing in the x -axis and just the residual fraction of the light on the edges is used for sensing along the y -axis.

It should be noted that any significant structure in the sodium column density (e.g., caused by a sudden bright layer, as occasionally seen) will be smeared out by a significant angular

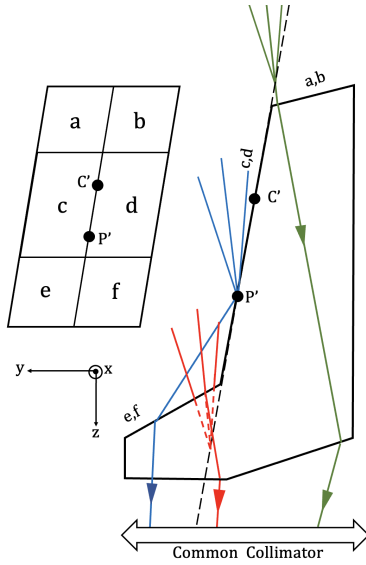


Fig. 4. Chief rays propagating through the 6 faces. A view from above reproducing the lettering of the surfaces is given in the upper left side.

width of the upwarding beam. The six-regions approach, in fact, deliberately does not make use of the eventual structures seen in the elongated LGS, as per different densities of the sodium layer.

Asymmetric solutions along the y -axis should be taken into consideration as well, recalling that the physical distribution of the sodium layer is generally asymmetric. Assuming that the layer “floats” above a certain height one can expect that the lower edge of the beacon will be sharper than the upper one (Ragazzoni et al. 2018). This would point toward solutions with a limited number of slicing regions, down to a minimum of three (Ragazzoni et al. 2019). In this configuration, only what is expected to be the sharpest edge is used to sense the derivative of the wavefront along the y -axis.

Figure 6 shows a possible arrangement for a six-pupil ingot, but a lot of other options are possible, resulting from different combinations of surfaces: 1) only reflective, 2) only refractive, 3) or a combination of both, depending on which region of the LGS image is being considered. The possible combinations of reflective and refractive surfaces mainly concern the implication of practicality. Provided that the inclination of the LGS focus on the focal volume is typical, a small perturbation with respect to the optical axis, making this surface refractive an unpractical solution, the adoption of, for instance, only reflective surfaces, would lead to the use of the collimator mainly off-axis. In the configurations we adopted, we qualitatively choose combinations that lead to chief rays of the various subapertures becoming elongated in opposite directions with respect to the optical axis. This choice is to make the specifications related to the quality of the collimating optics less demanding in terms of a useful FoV.

However, for any reasonable choice of splitting regions, the overall demand in terms of pixel format on the CCD is vastly smaller than any SH WFS (Ragazzoni et al. 2019) with a comparable spatial resolution on the WF. Considering a squared detector, let us note as N_p its side size in pixels. For a six-pupil configuration, arranged in a 2×3 format, we can easily estimate:

$$N_p \sim 3N, \quad (9)$$

where N is the number of subapertures along the diameter. The same estimation can be done for a SH WFS, by quantifying

N. OF FACES	LASER	PUPILS	DESIGN	SIGNAL			NOTES
				u	m	l	
6				xy	x	xy	
5				y	x	xy	$\beta_u = 0$
4a				y	x	y	$\beta_u = 0$ $\beta_l = 0$
4b				x(y)		xy	$\alpha_u = 90 - \alpha_m$
3				x(y)		y	$\alpha_u = 90 - \alpha_m$ $\beta_l = 0$ $d_l = 0$

Fig. 5. Possible configurations of the ingot prism. Column (1): Number of desirable faces. Columns (2)–(3): LGS sections and corresponding pupils. Note: the arrangement of the pupils is purely conceptual, the real position will depend on the considered optic implementation. Column (4): possible design of the prism. Column (5): signals that can be measured by considering the upper, medium and lower regions. Column (6): notes according to Fig. 7.

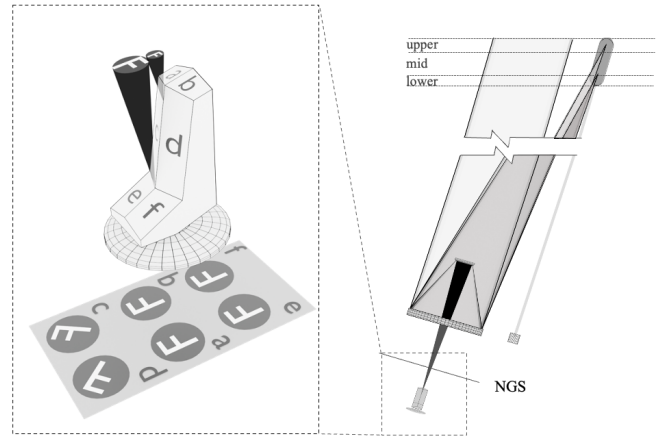


Fig. 6. Illustration of the telescope (right) together with the conjugation of the various layers of the sodium LGS beacon. The zoomed-in portion on the left shows the beams coming from the upper and lower portions of the artificial reference, together with the pupil rotations (highlighted by the “F” on the footprint of the pupils) because of the reflections and refractions through the ingot.

the largest elongation $\Delta\epsilon$ observed from the edge of the pupil opposite to the LGS launcher:

$$\Delta\epsilon \approx \frac{\Delta h}{h} \cdot \frac{D/2 + s}{h} \leq \frac{\Delta h_0}{h_0^2} \cdot D, \quad (10)$$

where the upper limit, occurring for zenith observations ($\theta = 0$), is calculated for the most favourable condition for the position of the projector ($s = D/2$).

If we consider the minimum apparent diameter of a non-elongated LGS propagated through a projector with perfect optical quality as $\sqrt{2}\epsilon_s$ (with ϵ_s being the seeing angle) and assuming a Nyquist sampling, a minimum subaperture size in pixels is given by:

$$\Delta_p = \sqrt{2} \frac{\Delta\epsilon}{\epsilon_s}. \quad (11)$$

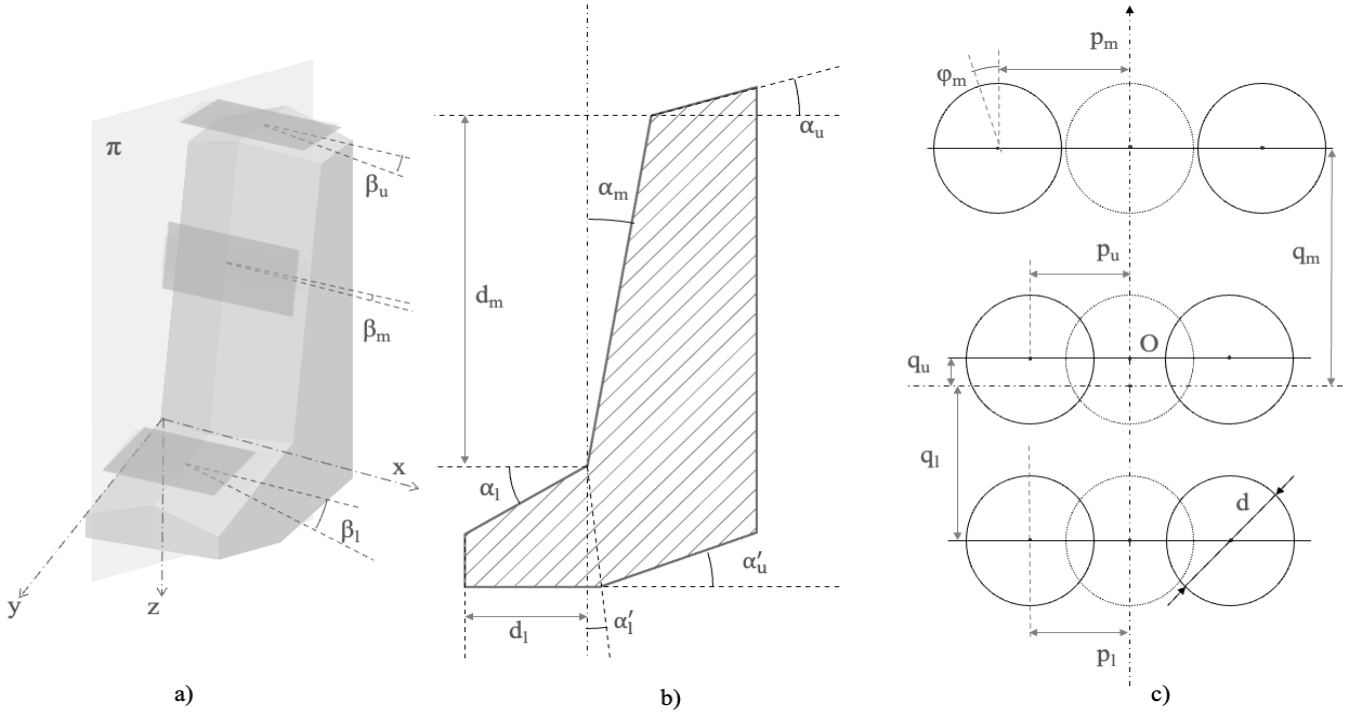


Fig. 7. Six-pupil ingot main characteristics. (a) Ingot prism solid shape with 6 faces. (b) Section of the prism. (c) 6 pupils corresponding to the 6 faces. u, m, l refer to upper, middle and bottom portions of the ingot.

Therefore, the overall detector format must be at least:

$$N_p \sim N \Delta_p. \quad (12)$$

Assuming $D = 40$ m, $\Delta h_0 = 20$ km and $N = 100$, for the ingot case, we get a result of $N_p \approx 300$ with respect to $N_p \approx 2100$ for the SH case, leading to a size ratio that is about seven times greater. This should be retained as a conservative estimate in favor of the ingot concept. In fact, such a ratio scales linearly with Δh_0 and increases as much as the LGS is being propagated away from the edge of the primary mirror, as in any practical case. It is interesting to point out that smaller detector formats are possible, as depicted in Agapito et al. (2022), where with $D = 39$ m, $N = 70$ and $N_p = 1100$ are adopted. This, however, is done at the expenses of handling in some manner an incomplete sampling of the LGS (truncation).

As a last consideration, we should take into account the fact that because of the cone effect, it is necessary to use this WFS scheme in a MCAO or similar system, so that the information per subaperture could come from different beacons. This means that a simple roof solution (not further explored here) could give satisfactory results with a large enough number of LGSs, despite it being unsatisfactory to completely resolve the wavefront information from a specific beacon.

3.1. Geometrical description

We consider the ray-tracing equations to describe the ray deviations operated by the faces of the ingot. When a ray with a direction $\hat{r} = (r_x; r_y; r_z)$ is reflected by a mirror with the normal to the surface having direction $\hat{n} = (\hat{n}_x; \hat{n}_y; \hat{n}_z)$, the direction of the reflected ray \hat{r}' is (Träger 2012):

$$\hat{r}' = M \cdot \hat{r}, \quad (13)$$

where the reflection matrix M is:

$$M = I - 2\hat{n} \cdot \hat{n}^T. \quad (14)$$

Then, I is the canonical identity matrix. The law of refraction can also be expressed in vector form and the direction of the refracted ray \hat{r}' is (Träger 2012):

$$\hat{r}' = \left\{ \sqrt{1 - \mu^2 [1 - (\hat{n} \cdot \hat{r})^2]} - \mu (\hat{n} \cdot \hat{r}) \right\} \hat{n} + \mu \hat{r}, \quad (15)$$

where:

$$\mu = \frac{n_1}{n_2} \quad (16)$$

is the ratio between the refraction indices for the incident (incoming) and transmitted (outcoming) mediums.

We go on to consider the case of a telecentric telescope with a chief ray propagating along the z direction: $\hat{r} = (0; 0; 1)$. We consider a mirror oriented perpendicularly to the incoming ray: $\hat{n} = (0; 0; -1)$. We rotate the mirror around x by an angle θ_x and we further rotate it around y by an angle θ_y . By applying the double rotation, the final orientation of the mirror will be:

$$\hat{n}' = R_x \cdot R_y \cdot \hat{n} = \begin{pmatrix} \sin \theta_y \\ -\cos \theta_y \sin \theta_x \\ -\cos \theta_y \cos \theta_x \end{pmatrix}, \quad (17)$$

where R_x and R_y are the rotation matrices around the x and y axes respectively. The reflection matrix associated with it is:

$$M = \begin{pmatrix} 1 - 2 \sin^2 \theta_y & 2 \sin \theta_y \cos \theta_y \sin \theta_x & 2 \sin \theta_y \cos \theta_y \cos \theta_x \\ 2 \sin \theta_y \cos \theta_y \sin \theta_x & 1 - 2 \sin^2 \theta_x \cos^2 \theta_y & -2 \cos^2 \theta_y \sin \theta_x \cos \theta_x \\ 2 \sin \theta_y \cos \theta_y \cos \theta_x & -2 \cos^2 \theta_y \sin \theta_x \cos \theta_x & 1 - 2 \cos^2 \theta_y \cos^2 \theta_x \end{pmatrix}. \quad (18)$$

The orientation of the ray after the reflection off the mirror is:

$$\hat{r}' = \begin{pmatrix} 2 \sin \theta_y \cos \theta_y \cos \theta_x \\ -2 \cos^2 \theta_y \sin \theta_x \cos \theta_x \\ 1 - 2 \cos^2 \theta_y \cos^2 \theta_x \end{pmatrix} = \begin{pmatrix} \sin 2\theta_y \cos \theta_x \\ -\sin 2\theta_x \cos^2 \theta_y \\ 1 - 2 \cos^2 \theta_y \cos^2 \theta_x \end{pmatrix}. \quad (19)$$

Referring to the upper, medium and lower part of the ingot as u, m, l , and calling $\alpha_m = 90^\circ - \theta_x$ and $\beta_m = \theta_y$, as shown in parts (a) and (b) of Fig. 7, we can rewrite the orientation of the reflected ray as:

$$\hat{r}' = \begin{pmatrix} \sin 2\beta_m \sin \alpha_m \\ -\sin 2\alpha_m \cos^2 \beta_m \\ 1 - 2 \cos^2 \beta_m \sin^2 \alpha_m \end{pmatrix}. \quad (20)$$

In the approximation of small angles, Eq. (20) becomes:

$$\hat{r}' \approx \begin{pmatrix} 2\beta_m \alpha_m \\ -2\alpha_m^2 \\ 1 - 2\alpha_m^2 \end{pmatrix}, \quad (21)$$

where such small angles are expressed in radians. It is worth noting that the central pupils (regions c and d in Figs. 4 and 6) due to the reflection are flipped and rotated by an angle, φ_m , given by:

$$\varphi_m \approx 2\beta_m \cos \alpha_m. \quad (22)$$

This is just a feature since they can be calibrated with an interaction matrix considering, for instance, modal bases. A similar approach can be used for the refractive faces. In this case, taking as an example the lower part of the ingot, characterized by the angle α_l , as indicated in Fig. 7, we can proceed as follows: 1) start from a refractive plane perpendicular to the z -axis: $\hat{n} = (0; 0; 1)$; 2) apply a rotation around x of $\theta_x = \alpha_l$ and a rotation around y of $\theta_y = \beta_l$ to find the orientation of the normal vector; 3) apply Eq. (15) consecutively for each refracting plane to calculate the ray vector exiting the ingot and 4) in the case of small angles the deviation of the ray can be expressed with the following simple relation:

$$\hat{r}' \approx \begin{pmatrix} (n-1)\beta_l \\ (n-1)\alpha_l \\ 1 - 0.5(n-1)(\beta_l + \alpha_l) \end{pmatrix}. \quad (23)$$

We note that at a first approximation, β_l and α_l are, respectively, the x and y component of the apex angle of the prism constituting the bottom part of the ingot. The first two components of \hat{r}' are basically the deviations operated by a thin prism with refractive index n , while the third component is the approximation of the normalization factor.

Using Eqs. (21) and (23), we can express the position of the pupils with respect to the optical axis (see Fig. 7 c) when they are reimaged by a lens with focal length, f_c :

$$\begin{aligned} p_m &\approx f_c[2\beta_m \alpha_m + (n-1)\beta_l]; & q_m &\approx f_c[2\alpha_m - (n-1)\alpha_l]; \\ p_u &\approx f_c(n-1)\beta_u; & q_u &\approx f_c(n-1)(\alpha_u - \alpha'_u); \\ p_l &\approx f_c(n-1)\beta_l; & q_l &\approx f_c(n-1)\alpha_l. \end{aligned} \quad (24)$$

Recalling that $d \approx f_c/F$, one can use, as a first approximation, the above equations to properly fit pupils into the chosen detector format in order to avoid overlaps and keeping a minimum guard distance among pupils to prevent scattering light from one pupil to the other. Those equations can be also used, of course, to properly engineer the detailed shape of the ingot in

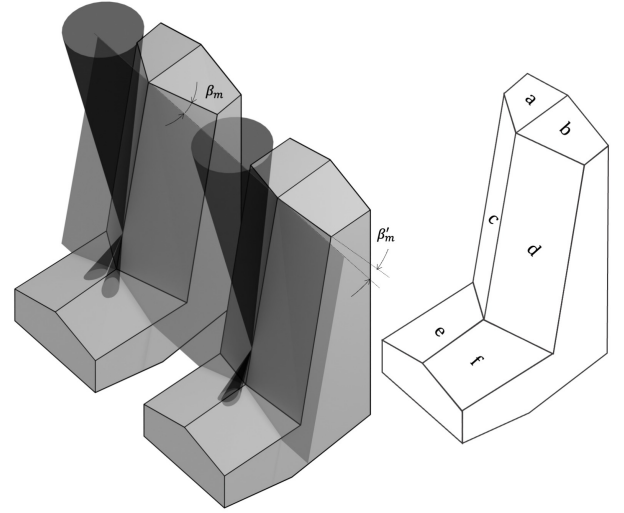


Fig. 8. Constraining the prism: the reflecting roof should exhibit a minimum angle, β_m , so that the reflection of the beams in the mid-part of the LGS source will be properly separated.

order to minimize deviations of the chief rays and second order effects like distortions of the pupil. It is worth pointing out that a detailed raytracing is needed in order to refine the final layout and given the monochromatic nature of the LGS, chromatism is not an issue at any degree of approximation, in contrast with the case of the pyramid WFS used with NGSs (Diolaiti et al. 2003). Negative values of the angles considered here should be taken into account in this optimization process, as it depends upon the particular focal ratio of the chosen telescope. Furthermore, the non-telescopicity of the telescope ought to be properly included, at least in the final ray tracing analysis.

It is to be noted that there are a few additional constraints. For example, as seen in Fig. 8, the angle, β_m , should be such that the beams reflected by faces c and d are separated at the level of faces e and f.

As Δh is continuously changing upon tracking, a further element is needed to define the ingot as an optical element, namely the “height” of such a component, d_m . This can be achieved through a number of methods, including a suboptimal application of the sensor, an anamorphic or conventional zoom optical relay to match the actual Δh with the reimaged length of a fixed ingot, or a variety of ingots with different heights. The solutions noted as 4b and 3 in Fig. 5 offer the practical advantage of allowing us to avoid this issue, although they (deliberately) neglect the use of one of the edges of the LGS source to get information on the derivative of the wavefront along the elongation.

3.2. An example of dimensioning the ingot prism

We take the example of an ELT to properly dimension a six-pupil ingot. The parameters used for the calculation are: the telescope diameter $D = 40$ m, laser launcher at $s = 21$ m from the telescope axis, focal ratio at the ingot: $F = 5$, and a telecentric beam.

The edge between the two reflective faces should be placed along the focal plane of the LGS, which forms an angle with the optical axis given by Eq. (8). This directly determines $\alpha_m \approx 6^\circ$. We further want the rays reflected by faces c, d to be separated at the level of faces e and f. This condition is met when the reflected chief rays are separated by at least the cone beam angle:

$$\arccos(\hat{r}'_c \cdot \hat{r}'_d) > 2 \arctan \frac{1}{2F}, \quad (25)$$

where \hat{r}'_c and \hat{r}'_d are the ray vectors reflected by the faces c and d respectively, characterized by the angles $\alpha_{m,c} = \alpha_{m,d}$ and $\beta_{m,c} = -\beta_{m,d}$. They can be found using Eq. (20) or, in the case of small angles, Eq. (21). In our case, we obtained $|\beta_m| > 36.5^\circ$ and, with the small angle approximation, subsequently $|\beta_m| > 39^\circ$.

The angles β_u and β_l can be easily found from Eq. (24), imposing the condition that the distance between the refracted pupils is equal or greater than the diameter. Assuming a refractive index of $n = 1.5$, we get $|\beta_{u,l}| > 11.5^\circ$. Consider now the relation for p_m in Eq. (24): if the first and second terms in the square brackets have opposite signs and similar amplitudes, they will cancel out and the pupils c and d will overlap. To avoid this, we can choose among two possibilities: In the first approach, we can choose β_l such that the x -component of the deviation generated by refraction adds up to the deviation generated by the reflective face. In this case, the lower faces of the ingot (e and f) will form a concave angle. This choice minimizes the angles of incidence and will result in a lower distortion of the pupil images, although the manufacturing of the prism will be likely more challenging and probably the device would be built by gluing together different optical blocks; In the second approach, we can choose β_l such that the x -component of the deviation generated by refraction compensates the deviation generated by the reflection. In this case, the term inside the square brackets shall be greater than half of the cone beam angle, meaning that β_l should be roughly twice the minimum value of 11.5° calculated above. This option will result in greater angles of incidence and thus higher distortions of the image pupils. The angle between faces e and f will be convex as the one shown in Fig. 7, leaving the option to build such a device as a single optical element.

We still need to find a proper value for α_l , α_u , and α'_u , all related to the vertical separation of the pupils. Since α_m is fixed by the LGS focal plane, and produces a deviation in the positive y direction, according to Fig. 7a, it is preferable to choose α_u and α'_u to produce an overall negative deviation. Moreover, to avoid vignetting of the rays refracted by the faces a and b, α_u should also produce a negative or close to zero deviation. We also note that q_m and q_l only differ for the term $2\alpha_m f_c$, which is always greater than the pupil diameter when the LGS launcher is outside of the telescope aperture; thus, any choice for α_l will keep a proper vertical spacing between the couples c, d, and e, f.

Finally, the choice of the angles $\alpha_u, \alpha'_u, \alpha_l$ is somehow arbitrary and deserves a short discussion. Of course, they are to be chosen to avoid superimpositions of the pupils. This is achieved by constraining the distances of the pupil to be greater than their diameter. Furthermore, an overall constant angle can be added to all the angles mentioned above, translating to a simple rigid translation of the pupil images in the detector plane. The detailed optimum choice should be achieved by minimizing the angles of incidence on the ingot faces in order to retain distortions of the pupil images to a minimum.

As a suboptimal example, choosing $\alpha_l = 0$, $\alpha'_u = -\alpha_u$ and imposing the minimum separation between the pupils a,b and e,f, we get $|\alpha_u| > 11.5^\circ$. Summarizing, a possible set of proper angles defining a six-pupil ingot for the ELT case described at the beginning of this subsection, can be individuated as:

$$\begin{aligned} \alpha_u &= 12^\circ = -\alpha'_u; & \beta_u &= 12^\circ = \beta_l; \\ \alpha_m &= 6^\circ; & \beta_m &= 40^\circ; \\ \alpha_l &= 0^\circ. \end{aligned} \quad (26)$$

3.3. Three-pupil ingot

In terms of number of reflecting interfaces and corresponding pupils, on the opposite side to the full six-pupil case described in

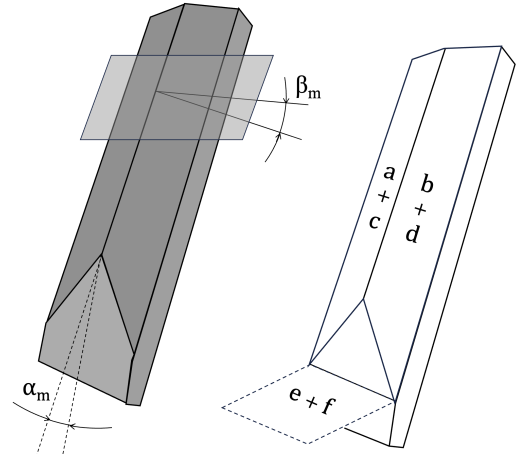


Fig. 9. Ingot prism solid shape in the case of three pupils. The pupils corresponding to e and f simply go unperturbed.

the previous subsection, it is worth addressing the simplest three-pupil situation (case “3” in Fig. 5). The practical implementation of this case is particularly advantageous as one of the interfaces (namely, faces e and f) is represented by the light going unperturbed without being reflected or refracted, while the other two interfaces are simple reflections (Fig. 9). Along with the “4b” case, this device is inherently compatible with any apparent LGS elongation, at the usual expense of sensing the derivative along y only using one of the edges of the LGS beacon. This edge is chosen as the sharpest end and is conjugated to the lower portion of the sodium layer, according to the statistics of the layer profiles and using the notion that the resonant molecules “float” over the atmosphere at a somehow well-defined height (Avila et al. 1998). In practical terms, in such a case, the ingot degenerates into a simple roof, which only should be truncated on one end to avoid the edges introducing some partial vignetting onto the reflected beams.

This will be characterized by a single angle, β_m , and using the relationships taken from the Eq. (24), we obtain:

$$\begin{aligned} p_m &= f_c [2\beta_m \alpha_m]; & q_m &= f_c [2\alpha_m]; \\ p_l &= 0; & q_l &= 0. \end{aligned} \quad (27)$$

Avoiding the pupil superimpositions and using the same $F=5$ telescope parameter as in the previous example translates into $\alpha_m = 6^\circ$ and $|\beta_m| > 36.5^\circ$. Although this approach is suboptimal for the measurements of the two derivatives along and orthogonal to the LGS elongation, its benefits are such that these configurations have been the focus of further tests and detailed studies. Obviously, appropriate choices of the parameters would improve the sensing, reducing the suboptimality to a marginal amount. A feasibility study for the three-pupil ingot, exploring its implementation on a large telescope and means to explore its sensitivity and resolution, has been carried out (Portaluri et al. 2022, 2023).

Furthermore, the three-pupil ingot has been subjected to laboratory testing (Di Filippo et al. 2021), in order to analyze experimentally its sensitivity (Radhakrishnan Santhakumari et al. 2020), by using a simulated LGS whose brightness distribution along the line of propagation can be properly adjusted to mimic the actual measurements (Gomes Machado et al. 2023). Low-order quasi-static aberrations measurable by such a WFS have been used to implement a tool to automatically align the

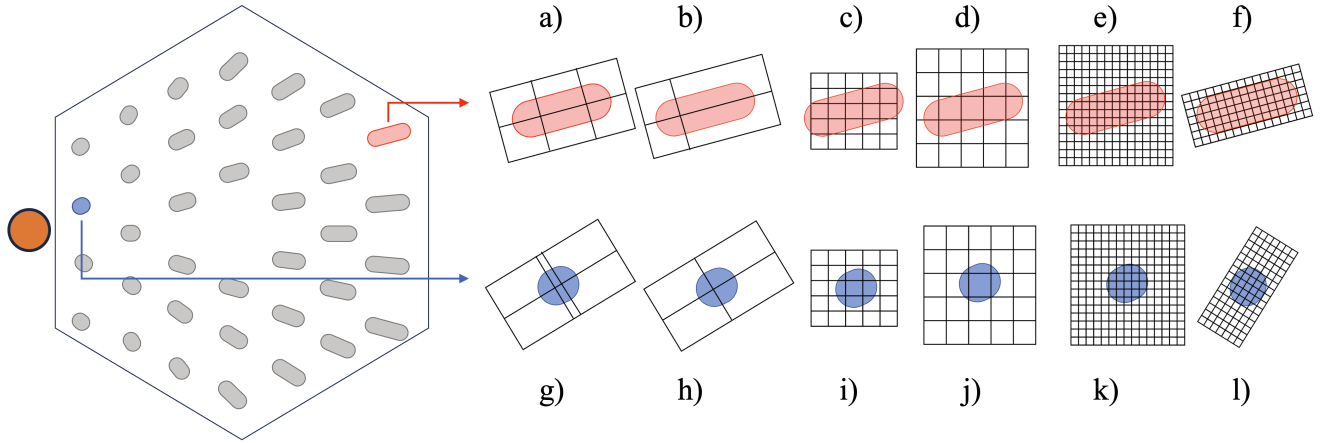


Fig. 10. Didascalical comparison among the ingot and SH WFSs used with an LGS fired alongside (propagated from the orange aperture left to the pupil) the hexagonal shaped telescope aperture. As the elongation varies across the entrance pupil, two cases of very mild (blue spots) and extreme (red spots) elongations are taken as representative in the six-pupil and three-pupil ingot configurations and for the SH approach. Of course, in the six-pupil ingot case, a single device is used but its projected elongation on the LGS pattern is inherently adjusted as depicted in cases (a) and (g), respectively; while cases (b) and (h) refer to the three-pupil ingot case. For the SH approach various examples are shown with nominal sampling as in (i), which could translate into the need for truncation as depicted in case (c) for a limited format detector. This can be overridden with coarse sampling as in cases (d) and (j) or with a large-format detector as in cases (e) and (k). The use of specifically designed polar detectors, briefly mentioned in the text, is outlined for cases (f) and (l) where of course the general case of an arbitrary angle between the pixel arrangement and the LGS elongation. It is clear that, as long as light distributions across the elongation is not used, the SH case is suboptimal with respect to the six-ingot case and the three-ingot case is lacking with respect to the former just along the elongated axis, y .

ingot to the 3D images of the LGS as collected by a simulated telescope in a real hands-on optical bench (Di Filippo et al. 2022). Actual closed-loop experimental simulations on an optical bench have also been carried out with a simplified model of the ingot (Arcidiacono et al. 2020).

Finally, purely numerical simulation tools have been developed (Viotto et al. 2018) to evaluate its performance (Portaluri et al. 2020a). This has been accomplished by using a hybrid approach between a pure ray tracing technique and a Fourier analysis (Viotto et al. 2020) and investigating different approximations of the LGS, by adopting several models for the ingot prism, and corresponding measurements of the slopes (Portaluri et al. 2020b). The code includes also the possibility of selecting three types of ingot: the six-, four-, and three-pupil configurations.

4. Conclusion

In this paper, we formalize the description of a new class of WFSs, nicknamed ingot WFS, which extends the pyramid WFS concept to an elongated LGS.

We defined several possible optomechanical options, ranging from three to six reimaged pupils and we explain the rationale behind computing the proper choice of the geometrical characteristics (angle and size) of the reflecting and refracting surfaces. We fully describe the ingot prism as an optical perturbator to be introduced at the reimaged volume, where an LGS is being focused on by a large telescope. Afterward, a common collimator would produce a number of pupil images that can be used in a linearized manner to estimate the derivative of the WF in the two axes.

The optimal use of the detector is one of the advantages that is fully retained with a pyramid-like WFS, and, above all, this is totally independent of the diameter of the telescope aperture. This makes the ingot WFS attractive for ELTs, especially if the lack of large-format detectors would lead to the need for truncation of the light, as may occur with the traditional SH WFSs.

Some of the several possible implementations and variations are particularly easy to carry out, accounting for only a minimum deterioration of the performance; the latter, of course, should be compared to the capabilities of other conventional WFSs used to sense LGSs. We recall that this new class of WFSs applies only to the cases where the LGS is propagated from outside the telescope aperture and, in fact, it complements an already existing family of WFSs (the z -invariant ones) that were similarly introduced for the case of an LGS being propagated from behind the cage of the secondary mirrors. They both describe a class of pupil plane WFSs aiming specifically to sense the atmospheric turbulence and taking into account the fact that the reference light comes from a source extended both on axial and lateral terms and considering the 3D nature of the LGS itself. This is in contrast with most of other approaches, where a WFS conceived for a natural reference star is being used in a suboptimal manner, to achieve sensing using only a portion of the light coming from different ranges with respect to the telescope.

The actual detailed computation of the sensitivity of such new class of WFSs is beyond the scope of this manuscript. However, we can easily note that the ingot approach is the pupil plane version of a SH-like WFS, where the spots are reimaged onto a pixel pattern that is aligned, per each subaperture, with the elongation of the LGS itself.

In order to qualitatively compare the ingot WFS sensitivity with respect of the SH case, we need to compare a number of different situations. With reference to the illustration depicted in Fig. 10, the case of the full six-faced ingot (also true for the case 4b) makes the ultimate use of the LGS light to sense the derivative along the x -axis. The three-pupil ingot would only underperform by the lack of a small portion of the light and it is likely to give comparable results. However, in both the cases of LGS truncation, the undersampling and of the non-aligned pixel pattern, it would clearly be expected to underperform. The exceptions occur if the whole ensemble of the LGS spots are aligned with the pixel pattern and the adoption of a sophisticated algorithm, maybe together by a finer sampling of the spot.

However, all these options lead to the need of an overall number of pixels of one or two orders of magnitude larger, if we consider an ELT-class telescope apertures. We do not speculate on the ensuing additional noise attributed to this pixel request (for example, the associated increase of readout noise). Along the y axis, the situation is, of course, radically different. If we plan to take advantage of the (evolving) structure of the light distribution along the LGS, this is clearly unattainable by the ingot concept. However, discarding this approach, the use of the light is almost optimal for the six-pupil ingot (along with the options 5 and 4a, with reference to Fig. 5) and, in the worst case, hampered by a factor two for the other configurations. As all these solutions have proper sense with large aperture and multiple LGSs are to be considered in any case, we should recall that the lack of derivative in one axes for a single LGS is usually constrained by the proper component of other LGS in any of the various MCAO or tomographic schemes.

The case of polar CCDs developed in the case of an LGS propagated from behind the cage of the obstruction of the telescope is well treated elsewhere (Thomas et al. 2008; Adkins 2012). In the case (described in this work) of an LGS fired from outside the pupil plane, the polar detector for a SH WFS would exhibit an asymmetric pattern as the center of the elongation would lie outside from the pupil area. It is reasonable, in fact, to assume that the ingot approach would get a similar level of sensitivity to such an approach, with the obvious advantages of a much more compact detector format (and the related consequences in case of a significant read-out noise). Further numerical and optical bench tests are ongoing, whereas testing on the sky would be an actual breakthrough for such an approach.

Acknowledgements. The authors would like to thank the Adaptive Optics group at the Laboratoire d'Astrophysique de Marseille for the several, very helpful discussions and to the anonymous Referee for several suggestions that greatly improved the manuscript. This study has been possible also with the help of ADONI, the Italian National Laboratory for Adaptive Optics and its related financial support. K.K.R.S. acknowledges support from the INAF Progetto Premiale "Optica Adattiva Made in Italy per i grandi telescopi del futuro". E.P. acknowledges the Osservatorio Astronomico di Padova for the hospitality while this paper was in progress.

References

- Adkins, S. M. 2012, *SPIE Conf. Ser.*, 8447, 84470R
- Agapito, G., Busoni, L., Carlà, G., et al. 2022, *SPIE Conf. Ser.*, 12185, 121858D
- Arcidiacono, C., Di Filippo, S., Greggio, D., et al. 2020, *SPIE Conf. Ser.*, 11448, 1144868
- Avila, R., Vernin, J., & Cuevas, S. 1998, *PASP*, 110, 1106
- Beckers, J. M. 1988, in *Very Large Telescopes and their Instrumentation*, ESO Conf., 2, 693
- Beckers, J. M. 1993, *ARA&A*, 31, 13
- Bharmal, N. A., Myers, R. M., & Yang, H. 2018, *SPIE Conf. Ser.*, 10703, 1070362
- Boyer, C., & Ellerbroek, B. 2016, *SPIE Conf. Ser.*, 9909, 990908
- Buscher, D. F., Love, G. D., & Myers, R. M. 2002, *Opt. Lett.*, 27, 149
- Butterley, T., Love, G. D., Wilson, R. W., Myers, R. M., & Morris, T. J. 2006, *MNRAS*, 368, 837
- Calia, D. B., Hackenberg, W., Holzlöhner, R., Lewis, S., & Pfrommer, T. 2014, *Adv. Opt. Technol.*, 3, 345
- Clare, R. M., Weddell, S. J., & Le Louarn, M. 2020, *Appl. Opt.*, 59, 6431
- Di Filippo, S., Greggio, D., Bergomi, M., et al. 2021, in *Adaptive Optics for Extremely Large Telescopes 6th Edition (AO4ELT6) Conference Series*, [arXiv:2101.07742]
- Di Filippo, S., Greggio, D., Bergomi, M., et al. 2022, in *Adaptive Optics Systems VIII*, 12185, eds. L. Schreiber, D. Schmidt, & E. Vernet, 121854V
- Dicke, R. H. 1975, *ApJ*, 198, 605
- Diolaiti, E., Tozzi, A., Ragazzoni, R., et al. 2003, *SPIE Conf. Ser.*, 4839, 299
- Diolaiti, E., Schreiber, L., Foppiani, I., & Lombini, M. 2012, *SPIE Conf. Ser.*, 8447, 84471K
- D'Orgeville, C., & Fetzter, G. J. 2016, *SPIE Conf. Ser.*, 9909, 99090R
- Ellerbroek, B. L. 1994, *J. Opt. Soc. Am. A*, 11, 783
- Esposito, S., & Busoni, L. 2008, *SPIE Conf. Ser.*, 7015, 70151P
- Esposito, S., Ragazzoni, R., Riccardi, A., et al. 2000, *Exp. Astron.*, 10, 135
- Esposito, S., Tozzi, A., Ferruzzi, D., et al. 2003, *SPIE Conf. Ser.*, 4839, 164
- Esposito, S., Riccardi, A., Fini, L., et al. 2010, *SPIE Conf. Ser.*, 7736, 773609
- Foy, R., & Labeyrie, A. 1985, *A&A*, 152, L29
- Foy, R., Migus, A., Biraben, F., et al. 1995, *A&AS*, 111, 569
- Fugate, R. Q., Ellerbroek, B. L., Higgins, C. H., et al. 1994, *J. Opt. Soc. Am. A*, 11, 310
- Genzel, R., Schödel, R., Ott, T., et al. 2003, *ApJ*, 594, 812
- Ghez, A. M., Salim, S., Weinberg, N. N., et al. 2008, *ApJ*, 689, 1044
- Gilmozzi, R., & Spyromilio, J. 2007, *The Messenger*, 127, 11
- Gomes Machado, T. S., Di Filippo, S., Bergomi, M., et al. 2023, in *Adaptive Optics for Extremely Large Telescopes 7th Edition (AO4ELT7) Conference Series*
- Gratadour, D., Gendron, E., Rousset, G., & Rigaut, F. 2010, in *Adaptive Optics for Extremely Large Telescopes*, 04005
- Guyon, O. 2018, *ARA&A*, 56, 315
- Hardy, J. W. 1998, *Adaptive Optics for Astronomical Telescopes*
- Herbst, T. M., Santhakumari, K. K. R., Klettke, M., et al. 2018, *SPIE Conf. Ser.*, 10703, 107030B
- Herrmann, J. 1992, *J. Opt. Soc. Am. A*, 9, 2257
- Horwitz, B. A. 1994, *SPIE Conf. Ser.*, 2201, 946
- Johns, M. 2008, *Proc. SPIE*, 6986, 698603
- Lombini, M., Schreiber, L., Diolaiti, E., & Cortecchia, F. 2022, *MNRAS*, 510, 3876
- Ma, X., & Wang, J. 2016, *Optik*, 127, 2688
- Macintosh, B. 2001, in *American Astronomical Society Meeting Abstracts*, 198, 83.04
- Marchetti, E., Hubin, N. N., Fedrigo, E., et al. 2003, *Adaptive Optical System Technologies II*, 4839, 317
- Marchetti, E., Brast, R., Delabre, B., et al. 2008, *SPIE Conf. Ser.*, 7015, 70150F
- Mayer, H. 1994, *Ophthalmic Res*, 26, 3
- Neichel, B., Rigaut, F., Vidal, F., et al. 2014, *MNRAS*, 440, 1002
- Pilkington, J. D. H. 1987, *Nature*, 330, 116
- Portaluri, E., Viotto, V., Ragazzoni, R., et al. 2017, *MNRAS*, 466, 3569
- Portaluri, E., Viotto, V., Ragazzoni, R., et al. 2020a, in *Adaptive Optics for Extremely Large Telescopes 6th Edition (AO4ELT6) Conference Series*, [arXiv:2012.09514]
- Portaluri, E., Viotto, V., Ragazzoni, R., et al. 2020b, *SPIE Conf. Ser.*, 11448, 1144831
- Portaluri, E., Di Filippo, S., Viotto, V., et al. 2022, *SPIE Conf. Ser.*, 12185, 121851K
- Portaluri, E., Radhakrishnan Santhakumari, K., Ragazzoni, R., et al. 2023, in *Adaptive Optics for Extremely Large Telescopes 7th Edition (AO4ELT7) Conference Series*
- Radhakrishnan Santhakumari, K. K., Greggio, D., Bergomi, M., et al. 2020, *SPIE Conf. Ser.*, 11448, 1144860
- Ragazzoni, R. 1996a, *ApJ*, 465, L73
- Ragazzoni, R. 1996b, *J. Mod. Opt.*, 43, 289
- Ragazzoni, R. 1997, *A&A*, 319, L9
- Ragazzoni, R. 2000, in *NATO Advanced Study Institute (ASI) Series C*, 551, Laser Guide Star Adaptive Optics for Astronomy, ed. N. Ageorges & C. Dainty, 125
- Ragazzoni, R. 2001, in *Science with the Large Binocular Telescope*, ed. T. Herbst, 13
- Ragazzoni, R. 2014, *SPIE Conf. Ser.*, 9148, 914811
- Ragazzoni, R., & Farinato, J. 1999, *A&A*, 350, L23
- Ragazzoni, R., Farinato, J., & Marchetti, E. 2000a, *SPIE Conf. Ser.*, 4007, 1076
- Ragazzoni, R., Giallongo, E., Pasian, F., et al. 2000b, *SPIE Conf. Ser.*, 4008, 439
- Ragazzoni, R., Tordi, M., Diolaiti, E., & Kirkman, D. 2001, *MNRAS*, 327, 949
- Ragazzoni, R., Diolaiti, E., Farinato, J., et al. 2002, *A&A*, 396, 731
- Ragazzoni, R., Kellner, S., Gaessler, W., Diolaiti, E., & Farinato, J. 2006, *MNRAS*, 368, 1796
- Ragazzoni, R., Viotto, V., Magrin, D., et al. 2013, in *Adaptive Optics for Extremely Large Telescopes 3th Edition (AO4ELT3) Conference Series*, eds. S. Esposito, & L. Fini, 33
- Ragazzoni, R., Portaluri, E., Viotto, V., et al. 2017, in *Adaptive Optics for Extremely Large Telescopes 5th Edition (AO4ELT5) Conference Series*
- Ragazzoni, R., Greggio, D., Viotto, V., et al. 2018, *SPIE Conf. Ser.*, 10703, 107033Y
- Ragazzoni, R., Viotto, V., Portaluri, E., et al. 2019, in *Adaptive Optics for Extremely Large Telescopes 6th Edition (AO4ELT6) Conference Series*
- Rigaut, F. 2002, in *European Southern Observatory Conference and Workshop Proceedings*, 58, 11

- Rigaut, F., & Gendron, E. 1992, [A&A](#), 261, 677
- Rigaut, F., & Neichel, B. 2018, [ARA&A](#), 56, 277
- Rigaut, F., Neichel, B., Boccas, M., et al. 2014, [MNRAS](#), 437, 2361
- Rodríguez-Ramos, J. M., Femenía Castellá, B., Pérez Nava, F., & Fumero, S. 2008, [SPIE Conf. Ser.](#), 7015, 70155Q
- Scheimpflug, T. 1904, Improved method and apparatus for the systematic alteration or distortion of plane pictures and images by means of lenses and mirrors for photography and for other purposes
- Schreiber, L., Diolaiti, E., Arcidiacono, C., et al. 2014, [SPIE Conf. Ser.](#), 9148, 91486Q
- Strehl, K. 1895, [Zeitsch. Instrumen.](#), 15, 362
- Szeto, K., Roberts, S., Gedig, M., et al. 2008, [SPIE Conf. Ser.](#), 7012, 70122G
- Thomas, S. J., Adkins, S., Gavel, D., Fusco, T., & Michau, V. 2008, [MNRAS](#), 387, 173
- Thompson, L. A., & Gardner, C. S. 1987, [Nature](#), 328, 229
- Tokovinin, A. 2004, [PASP](#), 116, 941
- Träger, F. 2012, [Springer Handbook of Lasers and Optics](#), 69
- Tyson, R. K. 1991, [Principles of Adaptive Optics](#)
- Vieira, L. E. L., Rodrigues Pipa, D., & Mello, A. J. T. S. 2018, [SPIE Conf. Ser.](#), 10772, 107720B
- Viotto, V., Bergomi, M., Portaluri, E., et al. 2015, in [Adaptive Optics for Extremely Large Telescopes 4th Edition \(AO4ELT4\) Conference Series](#), E34
- Viotto, V., Portaluri, E., Arcidiacono, C., et al. 2018, [SPIE Conf. Ser.](#), 10703, 107030V
- Viotto, V., Portaluri, E., Arcidiacono, C., et al. 2020, in [Adaptive Optics for Extremely Large Telescopes 6th Edition \(AO4ELT6\) Conference Series](#)
- Wilson, K. E., Lesh, J. R., Araki, K., & Arimoto, Y. 1997, [SPIE Conf. Ser.](#), 2990, 23
- Yang, H., Bharmal, N. A., & Myers, R. M. 2018, [MNRAS](#), 477, 4443
- Yang, H., Bharmal, N., Myers, R., & Younger, E. 2019, [J. Astron. Telescopes Instrum. Syst.](#), 5, 029002
- Zhang, Z., Morris, T., Bharmal, N., & Liang, Y. 2021, [Appl. Opt.](#), 60, 4208